Enhancing the Efficiency of Organic LEDs Through Spin-Orbit Coupling of Charge-Transfer States

by

Kelley Rivoire

Submitted to the Department of Physics
in partial fulfillment of the requirements for the degree of

Bachelor of Science in Physics

at the

MASSACHUSETTS INSTITUTE OF TECHNOLOGY

May 2006
[June 2006]

Author .....
Department of Physics
May 24, 2006

Certified by .....
Marc A. Baldo
Assistant Professor
Thesis Supervisor

Accepted by .....
David Pritchard
Thesis Coordinator, Department of Physics

Enhancing the Efficiency of Organic LEDs Through Spin-Orbit Coupling of Charge-Transfer States

by

Kelley Rivoire

Submitted to the Department of Physics
on May 24, 2006, in partial fulfillment of the
requirements for the degree of
Bachelor of Science in Physics

Abstract

In this thesis, the possibility of enhancing the efficiency of small molecule organic light-emitting diodes through spin-orbit effects is examined.

Because only singlet spin states, statistically one quarter of the total possible states, emit fluorescent light, it has generally been thought that a maximum of 25% efficiency could be attained without the addition of an emissive phosphor. Here, we present evidence that this is not a fundamental limit.

Two OLED structures have been studied, each providing evidence that the efficiency of the OLED can be enhanced by the use of a heavy-metal material to mix spin in charge-transfer states. A structure with a heavy-metal mixing layer placed beside a neat emissive layer was found to show a (2.5 ± 0.3) times enhancement in the efficiency compared with an OLED without the heavy-metal layer. However, differences in the electroluminescent emission spectra made attributing this result to spin statistics alone difficult. In a structure with the the heavy-metal mixing layer placed next to a fluorescent dye doped into a host, a (2.7 ± 0.2) times enhancement in the efficiency is measured.

Thesis Supervisor: Marc A. Baldo
Title: Assistant Professor

Acknowledgments

First and foremost, thanks to Professor Marc Baldo for offering me a chance – and then another when I didn't like the first one. But more than that, thanks for guidance with research, academics, and otherwise. Many thanks also are due to Michael Segal, who patiently answered what must have been an endless stream of dumb questions, and who never seemed to mind too much all those times I overslept. A big thanks also goes to everyone else in the Baldo group – Jon, Tim, Mike, Mihai, Kaveh, Benjie, Raja, and Kemal – for encouragement, friendship, and occasional manual labor.

No list of thank yous is complete without a mention of friends and family – and to mine, I'm quite grateful that they always believe in me, and somehow think I'm must smarter than I actually am. Finally, along with pretty much everything else in my life, this work is done with the memory of dad near to mind and heart.

Contents

List of Figures

Chapter 1

Introduction

One need only look at the recent density of journal citations, conference presentations, or faculty hires to notice the nascent revolution in organic electronics. While the past 50 years of electronics have been dominated by silicon materials, the latest boom is taking a step in another direction. Potentially huge payoffs loom – electronics based on organic materials could well slash the costs of fabricating and operating solid-state lighting and provide enticing possibilities of flexible electronics.

But there's more to this new technology than a flat-panel TV in every pot; organic electronics also provide a mine of interesting scientific questions and new regimes in which to probe them. The complicated molecules in organic materials present anything but a clean system for experimentation; the fundamental theories for these materials are a far cry from the precision of atomic physics, try as we might to adapt them.

Much of this thesis will be spent discussing spin statistics in the formation of singlet and triplet excited states of an electron-hole pair in small molecule organic light emitting devices. First, we will give a quick overview of organic LEDs, explaining their basic functionality and use. Next, the science behind the technology will be discussed, with a focus on fluorescence and phosphorescence mechanisms followed by a discussion of how the science affects the technology itself, namely in setting the efficiency. Then, experimental data demonstrating ways to modulate and increase the efficiency, based on the fundamental science in the system, will be presented.

before a final retrospective look at the work completed.

1.1 Organic LEDs

How does an organic LED function? One simple way to understand an organic light-emitting diode is to first consider a more traditional semiconductor light-emitting diode and then analogize. In solids, the energy levels are formed in bands; the highest filled band is called the valence band, and the lowest unfilled band is called the conduction band. In semiconductors, the gap between the two is not too large, about 1 eV, and it is possible to excite an electron into the conduction band.

If the semiconductor is doped, then its charge balance will be uneven. If the dopant atoms provide extra electrons, the material is n-type with electrons in the conduction level, and if it provides extra holes (the absence of an electron, which we can think of as a positive particle), it is called p-type and has holes in its valence band. If we put p and n type materials next to each other, electrons in the conduction band of the n-type material and holes in the valence band of the p-type material will recombine (Figure 1-1). If the gap of the material is chosen correctly, this recombination can generate a narrow band of light in the visible when forward biased (with cathode on the n-type material and current flowing from anode to cathode).

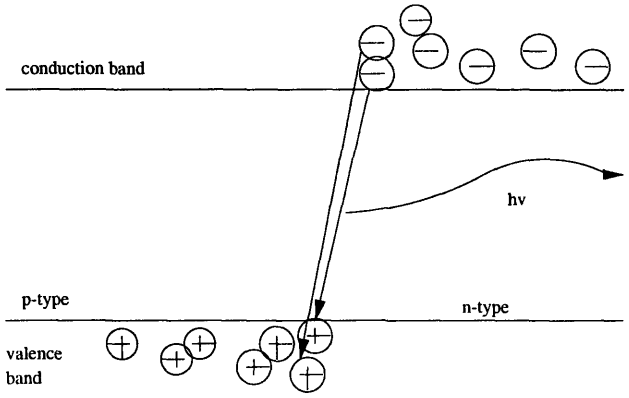

Figure 1-1: A schematic taken of a light-emitting diode. The right side is n-type; the left side is p-type. At the junction, electrons and holes recombine to emit light.

Now, we can take this basic model and apply it to organic materials with a few

key modifications. First, in organic materials electrons are not free, but bound in molecules. Fortunately, though, for the most part, it is only the outer orbitals (molecular orbitals that can be thought of as linear combinations of atomic orbitals) of a molecule that influence its optical and electronic properties. The highest occupied molecular orbital (HOMO) in a molecule acts quite similarly to a valence band; the lowest unoccupied molecular orbital (LUMO) acts similarly to the conduction band. Similarly to the situation in semiconductors, electrons in organics are carried in the LUMO and holes in the HOMO.

How do we drive electrons across a device? Instead of using a $p-n$ junction, we can use a heterostructure (first done by Tang and VanSlyke[40] in 1987) in which a material that transports holes well is placed next to a material that transports electrons well. Electrons are injected via a metallic cathode into the electron-transport layer (ETL) and holes from an anode into the hole-transporting layer (HTL). Assisted by the voltage applied across the device, electrons and holes are driven to the junction of the heterostructure, where it becomes energetically unfavorable for them to continue their voyage. The situation is again analogous to LEDs, and the carriers recombine and emit light (Figure 1-2).

But there is a difference in the recombination processes of LEDs and OLEDs; in organic materials, electrons and holes remain associated with molecules. As an electron in the HOMO and hole in the LUMO approach each other by various transfer processes, they begin to feel each other's presence and form a bound state, called an exciton. When this state exists across more than one molecule, it is known as a charge-transfer exciton (Figure 1-3). As the electron and hole continue to approach, the exciton transfers to a deeper bound intramolecular exciton, also called a Frenkel exciton. From this deeply bound state, the exciton can drop down to the ground state and emit fluorescent light.

Why are OLEDs potentially better than LEDs, or for that matter other types of lighting like liquid crystal displays or incandescent lights? Among their many advantages, organic LEDs are relatively easy to fabricate, operate at low voltage, consume relatively little power, and can be made extremely thin. Optimization of

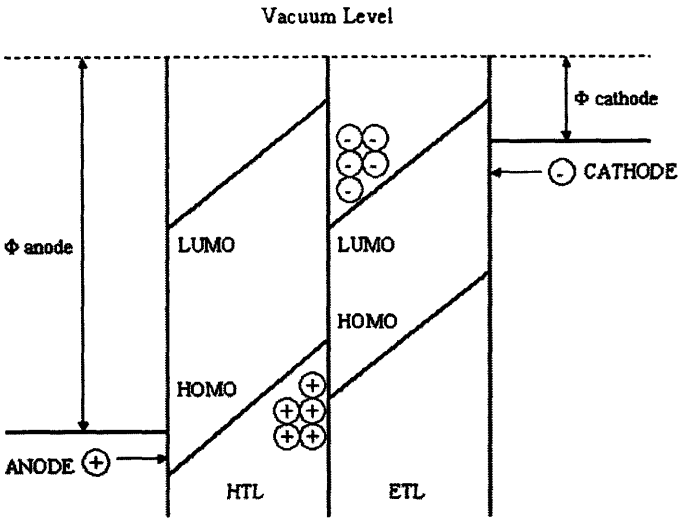

Figure 1-2: Basic schematic of a heterostructure OLED. Electrons and holes pile up at the junction of the heterostructure where they recombine, forming excitons that then decay and emit light. From [23].

OLEDs has the potential to significantly impact the lighting industry; already, it has made a dent, and commercial OLED products are widely available.

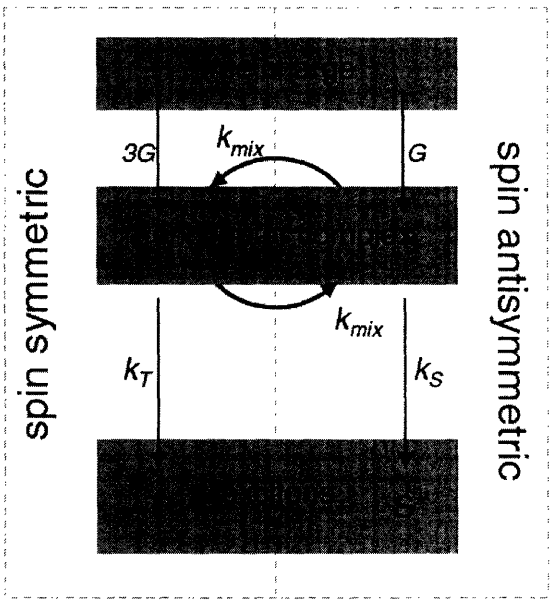

Figure 1-3: Model of exciton formation via separated charges then charge-transfer singlet and triplet states (in the "encounter complex"). Rates for each step are indicated on the figure; the rate k_{mix} shall be discussed in further detail in subsequent chapters. From [3].

Chapter 2

Physics of Two-Electron Systems

2.1 Spin in Two-Electron Systems

Since it is the bound electron-hole pair, or exciton, that is involved in the emission of light in an OLED, it is important that we understand the physics of such systems. We analogize with a discussion of spin in systems with two electrons (similar to the electron in the HOMO and a hole in the LUMO), as spin determines how light is emitted from the system. This section follows references [18, 16, 34, 4].

Spin statistics tell us that electrons, as spin-1/2 particles, are fermions, which have total wavefunctions that are antisymmetric under particle exchange; that is:

$$\Psi(\boldsymbol{r}_1, \boldsymbol{r}_2) = -\Psi(\boldsymbol{r}_2, \boldsymbol{r}_1) \tag{2.1}$$

The total electron wavefunction can be written as the product of the spatial and spin wavefunctions, $\phi(\boldsymbol{r}_1, \boldsymbol{r}_2)$ and χ respectively. Because the total wavefunction must be antisymmetric, there are two possible combinations of symmetry: 1) the spatial wavefunction is symmetric and then spin wavefunction is antisymmetric or 2) the spatial wavefunction is antisymmetric and the spin wavefunction is symmetric.

Now, let's consider the possible forms of the excited state spin wavefunction. The rules for addition of angular momentum tell us that for two spin-1/2 particles (each of which can individually be either spin up or spin down), the total spin may take on

integral values from $s_1 - s_2$ to $s_1 + s_2$, so either 0 or 1.

There are three possible ways to form a spin-one wavefunction, all symmetric under exchange:

$$\begin{aligned}\chi &= \uparrow(1)\uparrow(2)\\ \chi &= \frac{1}{\sqrt{2}}(\uparrow(1)\downarrow(2)+\downarrow(1)\uparrow(2))\\ \chi &= \downarrow(1)\downarrow(2)\end{aligned} \tag{2.2}$$

These are called the triplet states, they have quantum numbers m_s = 1, 0, and -1 respectively.

There is only one way to compose the singlet $s = 0$ (and $m_s = 0$) state:

$$\chi = \frac{1}{\sqrt{2}}(\uparrow(1)\downarrow(2)-\downarrow(1)\uparrow(2)) \tag{2.3}$$

Different symmetries of the spatial wavefunction also have implications. For a symmetric and antisymmetric two-electron spatial wavefunction ϕ_+ and ϕ_-, the interactions between the two electrons split them into two states with different energies; eigenenergies resulting from the interactions are:

$$\begin{aligned}E_+ &= \frac{e^2}{4\pi\epsilon_0}\langle\phi_+\left|\frac{1}{r_{12}}\right|\phi_+\rangle\\ &= \frac{e^2}{4\pi\epsilon_0}\langle\frac{1}{\sqrt{2}}\{a(1)b(2)+b(1)a(2)\}\left|\frac{1}{r_{12}}\right|\frac{1}{\sqrt{2}}\{a(1)b(2)+b(1)a(2)\}\rangle\\ &= J+K\\ E_- &= \frac{e^2}{4\pi\epsilon_0}\langle\phi_-\left|\frac{1}{r_{12}}\right|\phi_-\rangle\\ &= \frac{e^2}{4\pi\epsilon_0}\langle\frac{1}{\sqrt{2}}\{a(1)b(2)-b(1)a(2)\}\left|\frac{1}{r_{12}}\right|\frac{1}{\sqrt{2}}\{a(1)b(2)-b(1)a(2)\}\rangle\\ &= J-K\end{aligned} \tag{2.4}$$

where a and b are the individual electron spatial wavefunctions and J and K are

the 'Coulomb' and 'exchange' integrals defined as:

$$J = \frac{e^2}{4\pi\epsilon_0}\langle a(1)\, b(2) \left|\frac{1}{r_{12}}\right| a(1)\, b(2)\rangle$$
$$K = \frac{e^2}{4\pi\epsilon_0}\langle a(1)\, b(2) \left|\frac{1}{r_{12}}\right| a(2)\, b(1)\rangle \tag{2.5}$$

The electrons tend to be farther apart in an antisymmetric spatial configuration, so the energy of the antisymmetric spatial state (and symmetric triplet spin state) is lowered by a factor of $2K$ relative to the symmetric spatial state (and antisymmetric spin singlet state). This lowering will be important to the energetics and rates of transition for any operator that couples the two spin states.

Additionally, the triplet states can be split by the applying a magnetic field (the Zeeman effect).

2.2 Fluorescence and Phosphorescence

This section follows references [41, 4, 16]. To determine which types of two-electron states can emit radiation, we consider the dipole moment of the electron. For two states i and k, the transition dipole moment (the square of which is proportional to the transition probability) is:

$$\mu_{ik} = e\langle \psi_i(\boldsymbol{r}) \left|\boldsymbol{r}\right| \psi_k(\boldsymbol{r})\rangle \tag{2.6}$$

For a two-electron system, the dipole moment is:

$$\mu_{ik} = e\langle \psi_i(\boldsymbol{r}_1, \boldsymbol{r}_2) \left|(\boldsymbol{r}_1 + \boldsymbol{r}_2)\right| \psi_k(\boldsymbol{r}_1, \boldsymbol{r}_2)\rangle \tag{2.7}$$

The dipole moment should not change under exchange of two electrons, so only states of the same spatial symmetry can be coupled. Because of total wavefunction symmetry requirements, the spin symmetry of the wavefunction must also remain the same during a transition. The selection rule for spin is then $\Delta S = 0$.

The ground state of a molecule, as set by the Pauli principle, consists of orbitals

with paired electrons; therefore, it is a singlet state (S_0). Accordingly, the only transitions that can be made to the ground state are from excited singlets S_1; such transitions are called fluorescent and can be readily observed. Transitions from the excited triplet state T_1 to the ground state are forbidden by the spin selection rule.

But what happens when our initial excited state is not a well defined singlet? What if it also has some component of the triplet state? We can write this as

$$\psi = \chi_{S_1} + \lambda\chi_{T_1} \tag{2.8}$$

where λ is a parameter characterizing the mixing between triplet and singlet configurations. Following [41], from non-degenerate perturbation theory, we can approximate the mixing parameter

$$\lambda = \left| \frac{\langle \Psi_a | H | \Psi_b \rangle}{E_a - E_b} \right| \tag{2.9}$$

where Ψ_a and Ψ_b are the states being mixed and E_a and E_b are their energies. The likelihood of observing a spin transition will be proportional to the square of this parameter.

So for some interaction Hamiltonian that mixes the two states, as long as the energy separation between the states is not too large, a noticeable mixing can be observed, weakly allowing (with a relatively long lifetime) the forbidden excited triplet to ground state singlet transition. Similarly, the singlet excited state can drop down in energy to the excited triplet state as a result of this mixing, a phenomenon known as intersystem crossing.

What does process does this mixing correspond to physically? There are many interactions that have the capability to mix spin states, among them spin-orbit coupling, spin-lattice coupling, and hyperfine coupling. For the systems we are interested in, spin-orbit coupling is the most significant.

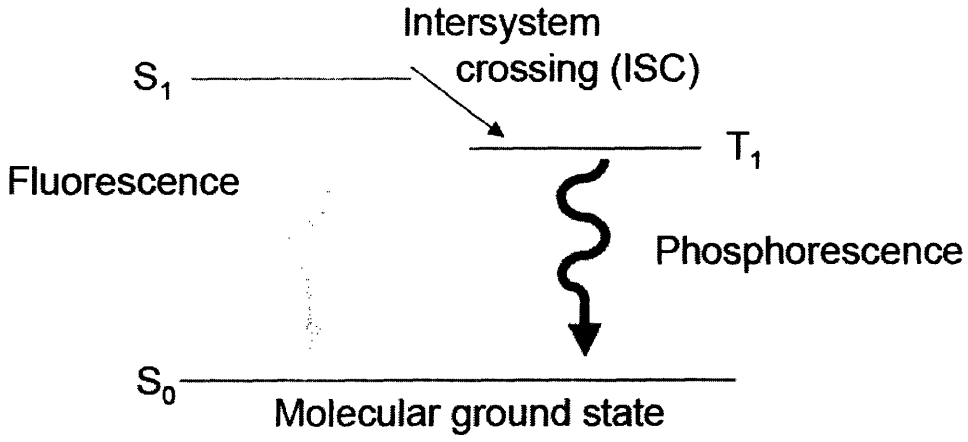

Figure 2-1: A schematic of intersystem crossing. Spin-orbit coupling allows forbidden transitions from the S_1 to T_1 state, followed by phosphorescence to the S_0 state. From [4].

2.3 Spin-Orbit Coupling

Spin-orbit coupling, arising from a field produced by the relative motion of electron and charged nucleus, is one of the many physical mechanisms that contribute to the complex spectral structure of atoms and molecules. But spin-orbit coupling does more than produce a pretty picture of line splittings. It is the spin-orbit interaction that allows mixing between singlet and triplet states – allowing the modulation of fluorescent and phosphorescent emission in OLEDs. And it is the quartic dependence of this interaction on the atomic number that allows us to strengthen the interaction through use of a heavy metal-containing molecule.

In this chapter, spin-orbit coupling will be described, from its simplest manifestation in the hydrogen atom, to the more complicated interaction in two-electron systems, including those surrounded by heavy metals.

2.3.1 Spin-Orbit Coupling in Hydrogen

The simplest example of spin-orbit coupling, and accordingly the textbook example learned by students in quantum mechanics classes, is in the hydrogen atom. This

section closely follows [1, 17, 2].

In hydrogen, spin-orbit coupling comprises one component of the fine structure – a set of corrections to the Bohr model that arise from relativistic effects. (The other components are labeled kinetic, referring to the correction between the classical and relativistic energies; and the Darwin term, which accounts for fluctuations in the electron's position of the same order as the Compton wavelength.)

In the reference frame of the electron, there is a motional magnetic field resulting from the proton, in SI units:

$$\boldsymbol{B}_{mot} = \boldsymbol{E} \times \frac{\boldsymbol{v}}{c^2} = -\frac{\boldsymbol{v} \times -\nabla\phi(r)}{c^2} \tag{2.10}$$

where $\phi(r)$ is the Coulombic potential from the nuclear charge, $\boldsymbol{B}$ is the magnetic field, $\boldsymbol{E}$ is the electric field, $\boldsymbol{v}$ is the velocity, r is the radius, and c is the speed of light.

Because the Coulombic potential is isotropic, $\nabla\phi = \frac{\boldsymbol{r}}{r}\frac{d\phi}{dr}$. The motional magnetic field simplifies to:

$$\boldsymbol{B}_{mot} = -\frac{1}{rc^2}\frac{d\phi}{dr}\boldsymbol{r} \times \boldsymbol{v} \tag{2.11}$$

Rewriting this in terms of the angular momentum, $\boldsymbol{l} = \boldsymbol{r} \times \boldsymbol{p} = m_e\boldsymbol{r} \times \boldsymbol{v}$, where $\boldsymbol{l}$ is the angular momentum, $\boldsymbol{p}$ is the momentum, and m_e is the mass of the electron, and $\boldsymbol{v}$ is the velocity, gives

$$\boldsymbol{B}_{mot} = -\frac{1}{m_e rc^2}\frac{d\phi}{dr}\boldsymbol{l} \tag{2.12}$$

For the Coulomb potential, $\phi = \frac{e}{4\pi\epsilon_0 r}$ is SI units, where e is the charge of the electron, and ϵ_0 is the permittivity of free space (note that this scales with Z for point charges of magnitude Ze),

$$\boldsymbol{B}_{mot} = -\frac{e}{4\pi\epsilon_0 m_e c^2 r^3}\boldsymbol{l} \tag{2.13}$$

To find the spin-orbit interaction, we need to find the Hamiltonian, $H = -\boldsymbol{\mu}\cdot\boldsymbol{B}_{mot}$,

where $\boldsymbol{\mu}$ is the magnetic moment of the electron. The magnetic moment is proportional to the spin, $\boldsymbol{\mu} = -\frac{e}{2m_e} g\boldsymbol{s}$ (which can be derived from the classical description of orbital angular momentum, along with the addition of a factor of two because of Thomas precession), and we approximate g for the electron as 2. This gives us the interaction:

$$\boldsymbol{H} = \frac{Ze^2}{8\pi\epsilon_0 m_e^2 c^2 r^3} \boldsymbol{l} \cdot \boldsymbol{s} \tag{2.14}$$

This interaction is more succinctly written

$$\boldsymbol{H} = \zeta(r) \boldsymbol{l} \cdot \boldsymbol{s} \tag{2.15}$$

where $\zeta(r) = \frac{Ze^2}{8\pi\epsilon_0 m_e^2 c^2 r^3}$. For hydrogenic orbitals, the expectation of r^{-3} goes like Z^3:

$$\langle \boldsymbol{r}^{-3} \rangle = \frac{Z^3}{n^3 a_0^3 l \left(l + \frac{1}{2}\right)(l+1)} \tag{2.16}$$

where $a_0 = \frac{4\pi\epsilon_0 \hbar^2}{m_e^2 e^2}$ is the Bohr radius, and n and l are the principal and angular momentum quantum numbers, respectively, such that we can write

$$H = \frac{\alpha^2 R_H Z^4}{n^3 l \left(l + \frac{1}{2}\right)(l+1)} \tag{2.17}$$

with the fine structure constant, $\alpha = \frac{e^2}{4\pi\epsilon_0 \hbar c}$, and the Rydberg constant $R_H = \frac{m_e e^4}{8\pi\epsilon_0^2 h^3 c}$.

With these relations, we find that the spin-orbit Hamiltonian scales like the fourth power of the mass number Z, meaning that the relative strength of the spin orbit coupling is much stronger in heavier atoms and molecules.

2.3.2 Changes in Spin Multiplicity via Spin-Orbit Coupling

When two electrons are involved in our system, we find that each has a spin-orbit term. Following [2], we can sum their contributions to the Hamiltonian:

$$H_{so} = \sum_{i=1}^{2} \zeta_i \boldsymbol{l}_i \boldsymbol{s}_i \tag{2.18}$$

This can be written as a sum of the $\boldsymbol{s}_1 + \boldsymbol{s}_2$ and the $\boldsymbol{s}_1 - \boldsymbol{s}_2$ operators:

$$\boldsymbol{H}_{SO} = \frac{1}{2}(\zeta_1 \boldsymbol{l}_1 + \zeta_2 \boldsymbol{l}_2) \cdot (\boldsymbol{s}_1 + \boldsymbol{s}_2) + \frac{1}{2}(\zeta_1 \boldsymbol{l}_1 - \zeta_2 \boldsymbol{l}_2) \cdot (\boldsymbol{s}_1 - \boldsymbol{s}_2) \tag{2.19}$$

Since $\boldsymbol{s}_1 + \boldsymbol{s}_2$ commutes with the total spin operator $\boldsymbol{S}^2$, it preserves the total spin. On the other hand, $\boldsymbol{s}_1 - \boldsymbol{s}_2$ allows transitions between spin states.

For example, for the z-component of spin-orbit coupling:

$$(s_{1z} - s_{2z})\,|0,0\rangle = \hbar|1,0\rangle \tag{2.20}$$

so that there is a coupling between the $|0,0\rangle$ and $|1,0\rangle$ states:

$$\langle 1,0|H_{SO}|0,0\rangle = \frac{\hbar}{2}(\zeta_1 l_{1z} - \zeta_2 l_{2z}) \tag{2.21}$$

meaning that it is possible to convert spin singlets into spin triplets and vice versa. Overall angular momentum must be conserved in a transition, so by coupling the orbital and spin angular momenta, we make possible a spin transition.

The possibility for a spin-flip can also be described visually as in [41], through spin cones, with the spin vectors from the two electrons either in phase (for triplets) or 180 degrees out of phase (for singlets).

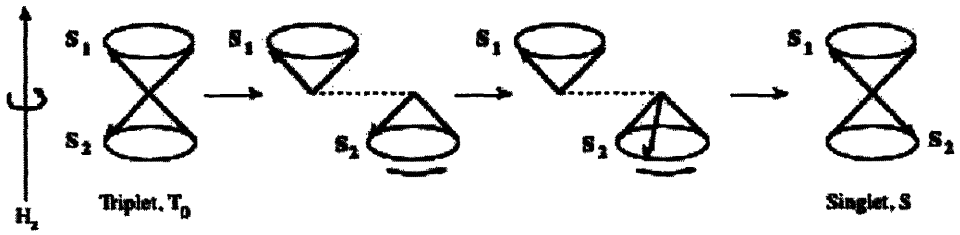

Figure 2-2: A schematic of a spin change. The two electrons feel different magnetic fields, causing the electron represented by the lower part of the cone to precess about the $\hat{z}$ axis at a faster rate, allowing the transition from triplet to singlet. From [41].

Because spin-orbit coupling represents an internal magnetic field, the spin precesses about this field at a constant tipping angle, in accordance with the classical picture of angular momentum and torque. We can define the field to point in the

$\hat{z}$ direction. Then the spin vector precesses about the field at the Larmor frequency $\Omega_L = -\gamma B$, where γ is the gyromagnetic ratio, and B is the magnitude of the field – this precession depends on the field.

But the internal field seen by the two electrons varies because they are spatially separated; they precess about the field with different rates, meaning that there is a relative dephasing. Following Figure 2-2, a spin triplet in the T_0 (triplet with $m_s = 0$) state is transformed into a spin singlet after a relative phase difference of π is accumulated between the two spins. In the absence of an external field, the zero-field splitting separating the three triplet states is small, and we can think of the triplet states as degenerate.

The spin dephasing allowed through the spin-orbit coupling cannot be reproduced with a uniform external magnetic field: it is the spatial variation that allows phase differences to accumulate and transform spin states. The application of an external field, would however, split the three triplet states (the Zeeman effect).

Chapter 3

Efficiency in Organic LEDs

3.1 Factors Influencing Efficiency

For organic LEDs to be a viable technology, they must demonstrate high efficiency. It's worthwhile, then, to examine the factors that influence efficiency and look at which ones can be easily increased.

The electroluminescent efficiency can be thought of most simply as the amount of light emitted divided by the current fed into the device to produce electrons and holes. This efficiency can be written as the product of four major factors:

$$\eta_{EL} = \gamma \eta_{fl} \chi_s \eta_{out} \tag{3.1}$$

where η_{fl} is the efficiency of fluorescent radiation from the S_1 state to the S_0 state; γ is the fraction of injected charges that form excitons, χ_S is the fraction of excitons formed in the singlet state, and η_{out} is the fraction of light coupled out of the device. A detailed look at each of these contributors can be found in [32].

The outcoupling efficiency, η_{out}, is the result of internal reflection and absorption that prevents radiation from exiting the device and entering a detector (Figure 3-1). This is given in [4] as approximately 20 percent. Aligning the emitting dipoles inplane and shifting the recombination zone to an optimal location have been found to improve the outcoupling; it is cited in [32] as being as high as 50 percent in some

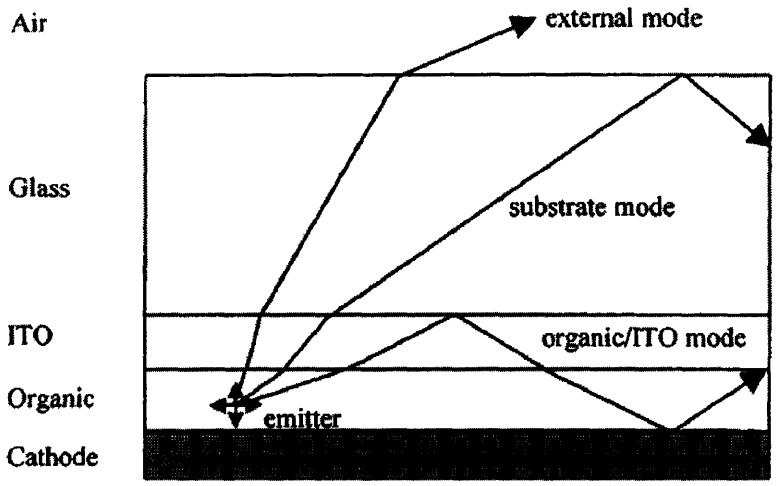

Figure 3-1: A schematic showing efficiency losses due to waveguiding inside the device. Indium tin oxide (ITO) is used as the conductive anode. From [32].

cases.

The fluorescent efficiency η_{fl} measures how effectively excited singlets emit light compared with loss to nonradiative processes. By optimizing the material, this efficiency can be made quite high [4, 32, 28].

The fraction of injected charges that form excitons, γ, can be made close to unity through the use of multiple layer devices that prevent electrons and holes from leaking across the device without recombining.

Finally, we are left with the singlet fraction χ_s.

3.2 Measurements of the Singlet Fraction in Small Molecule and Polymer OLEDs

Elementary spin statistics point to χ_s being 25% because singlets account for one quarter of the possible spin states. This has been verified and is generally accepted in small molecule emitters[7] though this thesis will look at whether it is possible to modulate this quantity in the presence of a spin mixer. Much more controversial have been measurements on polymer organic LEDs, discovered in 1990[14].

Indirect measurements of χ_S for polymers were first found to exceed 25% percent and approach 50%[15] in 1999. Since others[44], have found similar results, some by more direct measurements[43] of χ_s, though the result has not been universally reproducible[38] and some of the techniques used to make these determinations have been questioned[38, 30].

Theoretical and experimental work has shown that such a high value of χ_S in polymers is possible[13, 26, 22, 25, 39, 45, 11, 27], though the justification varies from author to author, and even paper to paper by the same author. One oft-suggested possibility is that the singlet and triplet states, either excitons[13, 22] or charge-transfer states[27, 28, 26], might be separated by a small enough exchange splitting that the reverse intersystem crossing k_{TS} from the triplet state to the singlet state might not be hampered too much by energetics (because $k_{TS} = k_{ST}e^{-\frac{\Delta E}{kT}}$, where ΔE is the splitting, T is the temperature and k is Boltzmann's constant). If the transition out of the associated singlet state (either charge-transfer or exciton) happens relatively quickly compared with transitions out of the associated triplet state, then this would allow χ_S to exceed 0.25. In [26], the CT singlet-triplet separation was measured to be 3-6 meV, less than kT, for ladder-type polymers.

A larger rate of transition for singlet states than triplet states is consistent with a larger formation cross-section for singlets, which was predicted theoretically[11, 39]. It has also been suggested[11] that the closer the singlet CT state is to the singlet exciton, the higher the singlet exciton formation rate will be compared to the triplet formation rate, allowing the possibility of χ_S exceeding 0.25 with the addition a mixing element. The singlet CT state is close to the singlet exciton in long-chain polymers in which χ_S has been measured above 0.25, according to [27, 11], while small molecules that show $\chi_S \simeq 0.25$[11] have a larger energy difference between singlet CT state and exciton.

Other suggested explanations include that a better match between the ionic character of singlet CT and exciton states than of triplets leads to faster singlet exciton formation[25, 45] or that for large exchange energy, a phonon bottleneck slows the formation of triplet excitons[22]. However, as noted in [3], a difference in formation

rates alone cannot change χ_S; there must also be a mixing element between singlets and triplets to make use of the advantageous relative formation rates. [33] cautions that such a mixing element necessary for nonzero k_{TS} is not inherently available in all systems and must perhaps be induced by means of a heavy-atom element and moreover questions the validity of the result in [44] because the system lacked a mixer (systems in [43] did, however, include such a mixer, [33] notes).

3.3 Triplet Harvesting

Regardless of the value of χ_S, however, it is possible to attain a higher luminescent efficiency from OLEDs by employing a phosphor doped into the emissive layer to harvest triplets from which no light would otherwise be produced [8]. Because of intersystem crossing, singlets formed on the fluorescent material will also transfer to the phosphor and emit via phosphorescence.

3.4 Sensitized Fluorescence

Additionally, a phosphor can be used to allow a fluorescent dye to emit both singlet and triplet excitons by doping a both a fluorescent dye and a phosphor into the emissive layer. In this process, called sensitized fluorescence (Figure 3-2) triplet excitons formed on the host and transferred to the phosphor by intersystem coupling can then transfer to a fluorescent dye where they emit fluorescence. This mechanism has been tested by measuring the lifetime of the fluorescent light; it was found to track with the much longer lifetime of the phosphor rather than the much shorter fluorescent lifetime[10].

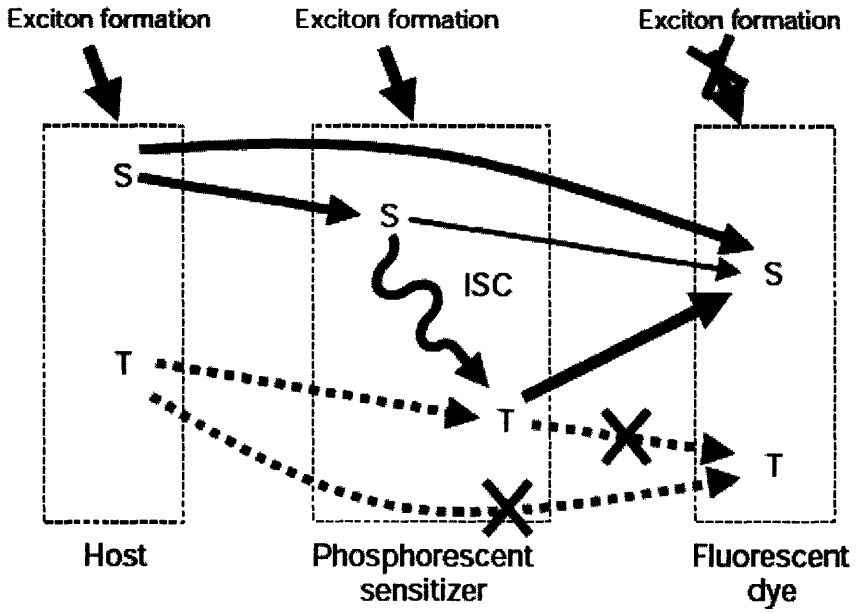

Figure 3-2: Diagram demonstrating pathway for sensitized fluorescence. From [10].

Chapter 4

Experimental Methods

In the experiments described in the next sections of this thesis, a few key experimental methods are used; the basic methods are described here. Thermal evaporation is used to deposit organic thin films; photoluminescence and electroluminescence are measured for organic LEDs made from these thin films.

4.1 Thermal Evaporation

Thin films of organic materials are deposited onto a glass substrate via the method of thermal evaporation (Figure 4-1). The materials to be deposited are placed inside a vacuum chamber operated with a base pressure of 10^{-7} torr. The chamber is pumped by the combination of a turbo pump and a cryo pump. The materials are placed inside the chamber inside heat-resistant metal boats. At low pressure, a voltage is applied across the resistive boat, heating the material inside until it begins to evaporate at a slow and controlled rate on the order of $1\mathring{A}$ per second. The substrate is held in place at the top of the chamber in a direct path of the source boat such that the material evaporates onto it.

The thickness of the layer and accordingly the rate of deposition are controlled by a quartz crystal microbalance. The piezoelectric crystal is driven by an AC current at its resonant frequency, which causes the crystal to oscillate. The resonant frequency can be measured with great sensitivity; this frequency will change according to the

Sauerbrey equation[35] as mass is deposited onto the active area of the crystal:

$$\Delta f = -C\frac{f_0^2 \Delta m}{A} \tag{4.1}$$

where f is the crystal frequency, f_0 is the resonant frequency, Δm is the added mass, A is the active area, and C is a constant dependent on the crystal.

The substrates are fabricated on glass slides precoated with 1600Å-thick layers of transparent and conductive indium tin oxide (ITO). The ITO surface is solvent-cleaned and then exposed to ozone and UV radiation for 5 minutes. To planarize the ITO, poly(3,4 ethylenedioxythiophene):poly(4-styrenesulphonate) (PEDOT:PSS) is spun onto its surface and baked at 115 C for a minimum of 30 minutes.

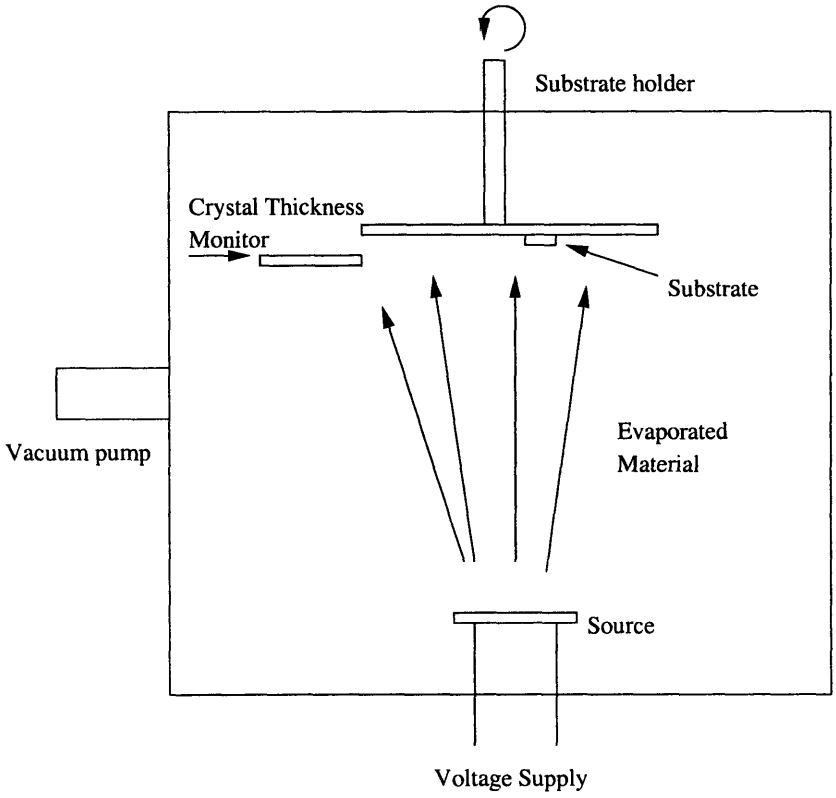

Figure 4-1: A schematic of the thermal evaporation system. Material form the bottom of a chamber is heated by applying a voltage to its resistive container. A quartz crystal microbalance measures the deposition rate and thickness.

4.2 Photoluminescence

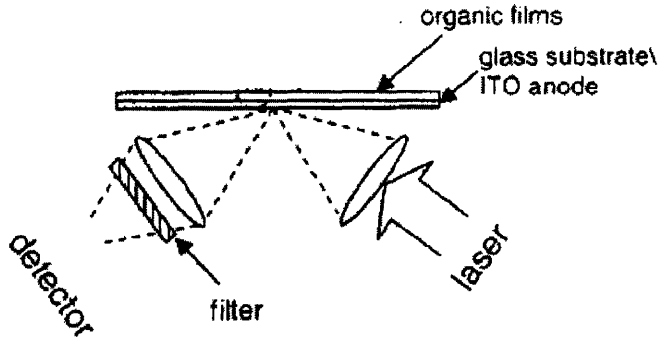

Figure 4-2: Block diagram of photoluminescence measurement. Adapted from [38]

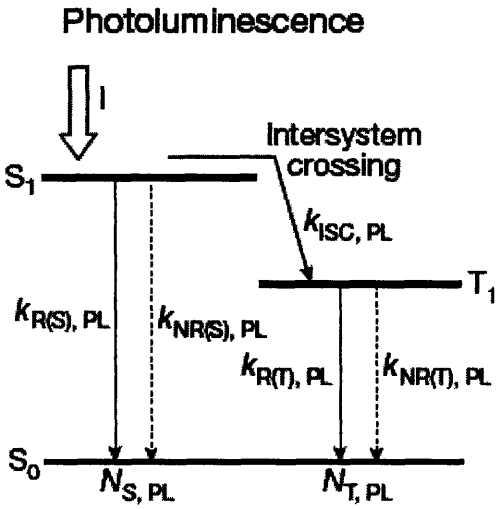

Figure 4-3: Laser light is absorbed into the S_1 state. In the presence of a mixing element, intersystem crossing takes place, followed by phosphorescence. Diagram labels rates of radiative and nonradiative transitions originating from the S_1 state. N designates the efficiency. From [43].

In photoluminescence, light, in this case a 408 nm laser, is directed onto a set of organic thin film layers deposited on glass (Figure 4-2). The light is absorbed directly into the S_1 excited state and then decays back to the S_0 state, emitting light that is measured by a photodiode coupled to a spectrophotometer with a monochromator

and cooled CCD. In the presence of a mixing phosphor, intersystem crossing from the S_1 to the T_1 state can occur, followed by phosphorescence that will also be measured (Figure 4-3). To avoid measuring the laser pump itself, a filter is placed in front of the photodiode to screen out light of the pump wavelength (which differs from the wavelength we are interested in measuring).

4.3 Electroluminescence

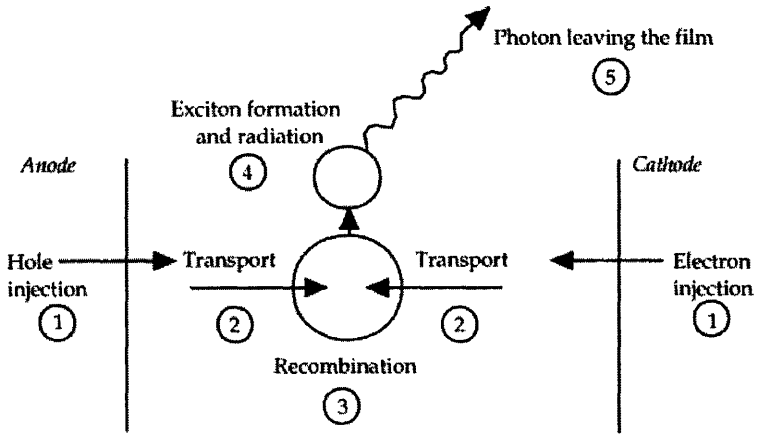

Figure 4-4: Basic diagram of electroluminscence showing charge injection, charge transport, recombination, exciton formation, and emission. From[36].

In electroluminescence (EL), charges, rather than photons as in PL, eventually produce the excitons. Charges (holes from the anode and electrons from the cathode) are injected by tunneling and thermionic emission[37]. They are then transported from molecule to molecule by hopping processes before they reach the junction of the heterostructure where they are trapped and recombine, forming excitons and emitting light (Figures 4-4, 4-5). More on charge injection and transport in OLEDs can be found in [37, 6].

Electroluminescent efficiency is measured by scanning across voltages and recording the current and light output using a parametric analyzer. A spectrum of the light emission can taken at any voltage using the spectrophotometer system.

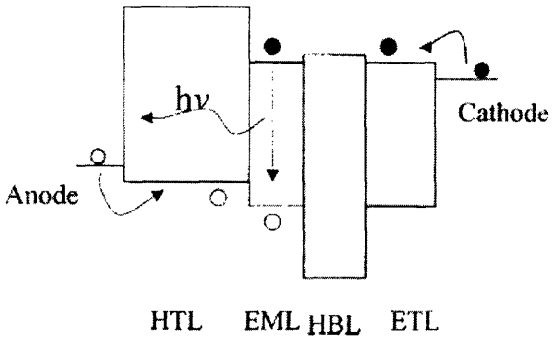

Figure 4-5: Holes are transported from the anode across the hole transport layer (HTL); electrons are carried from the cathode across the electron transport layer (ETL). A hole-blocking layer prevents holes from crossing into the HTL and forces recombination to happen in the emissive layer (EML). From[24].

Chapter 5

Generating an Efficiency Enhancement

With the elements of the electroluminescent process now established, the challenge is to find a way to increase the efficiency, namely through χ_S, the singlet fraction. All of our experiments are made with small molecule OLEDs, where the singlet fraction is generally accepted to be 0.25 (as opposed to in polymer OLEDs where there have been measurements of χ_S exceeding this number).

We start with the model in Figure 5-1, which shows the relevant charge-transfer and molecular exciton states and their rates of generation. The goal of the experiments described will be to test the validity of possible paths that would increase lead to χ_S exceeding 0.25. One possible pathway requires: the rates of mixing between CT states, k_X^{TS} and k_X^{ST}, be comparable to the rates of singlet and triplet exciton generation, k_S and k_T, and either 1) k_X^{TS} exceeds k_X^{ST} or 2) $k_S \gg k_T$, something that has been theoretically predicted for polymers[39, 25], but has not been tested with such scrutiny in small molecules.

But because the end result is to increase fluorescent emission, we also want to minimize k_{ISC}, which results in a relative increase in phosphorescent emission compared to fluorescent emission. This seems to be at odds with the requirement that k_X^{TS} be non-negligible; however, because CT states form with the electron and hole much farther apart than in the exciton, it may be possible to spatially separate the

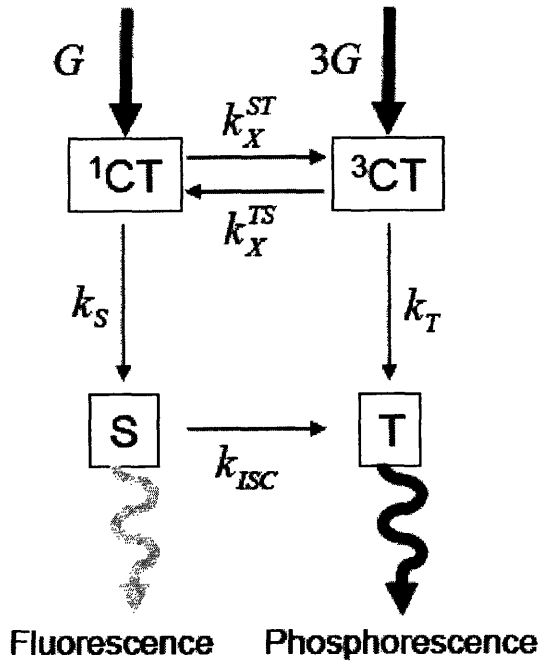

Figure 5-1: A model describing the formation of excitons in electroluminescence. G and $3G$ describe the relative rates of formation for charge-transfer excitons from uncorrelated pairs of charges; this is assumed to be determined by spin statistics. Rates k_X^{TS} and k_X^{ST} label the mixing rates between the CT states; depending on the splitting of the CT state, these could be quite different. k_{ISC} is the intersystem crossing between the exciton singlet and triplet; because the exciton splitting is known to be large in small molecules with singlet higher than triplet, the reverse process is not relevant.

effects of a phosphor on k_X^{TS} and k_{ISC}.

We then construct device structures based on this principle of trying to maintain a large k_X^{TS} while minimizing k_{ISC}. One such general structure is to build, from the substrate up: anode, hole-transporting layer, emissive fluorescent layer, mixing electron transport layer, hole blocking layer, cathode. The idea behind this structure is that electrons would be transported from the cathode across the hole blocking layer and mixing layer to the emissive layer, while holes would be transported from the anode across the HTL to the emissive layer. Charge-transfer states would form from the combination of a mixed electron in the mixing layer and holes in the emissive

layer. With the materials chosen so that the exciton in the emissive layer has lower energy than the exciton in the mixing layer, excitons would form in the emissive layer, sufficiently far from the mixing phosphor to avoid a large k_{ISC} and lower fluorescent efficiency.

To test this possible pathway for exciton formation, we build an OLED with indium tin oxide as the anode, 500$\AA$ TPD as the HTL, 50$\AA$ DCM as emissive layer, 150$\AA$ FIrpic as a mixing electron transport layer, 200$\AA$ BCP as the hole blocking layer, and 12$\AA$ Lithium Fluoride/1000$\AA$ Aluminum as the cathode on a glass substrate. Full chemical names and detailed structures for the organic materials can be found in Appendix A. The DCM layer is purposefully made thin to pin down the exact location where recombination occurs. To test whether this device structure has increased efficiency as a result of high χ_S, we compare its efficiency with that of a device in which the 150$\AA$ of FIrpic and 200$\AA$ of BCP is instead replaced by 350$\AA$ BCP. Both structures have the same device thickness to prevent microcavity effects[12] from influencing the emission.

Measurements from three devices with the mixing layer give external quantum efficiencies of (0.35 ± 0.04), where the error is calculated solely from an unweighted average of the three measurements. For three devices with the thicker ETL and no mixing layer, the efficiency is measured to (0.141 ± 0.002). The ratio of efficiency between the two sets of devices is then (2.5 ± 0.3), which we interpret to suggest that χ_S is the system may exceed 0.25.

5.1 Electroluminescent Spectra

To ensure that the light we measure is generated from excitons in the emissive layer, we can measure a spectrum at a given voltage and match this to the characteristic emission of the fluorophore. Electroluminescent spectra for devices with and without the mixing layer peak at different wavelengths, as polar molecules are known to have spectra that shift depending on their local environment and concentration[9].

The spectral differences could be the result of varying contributions from two

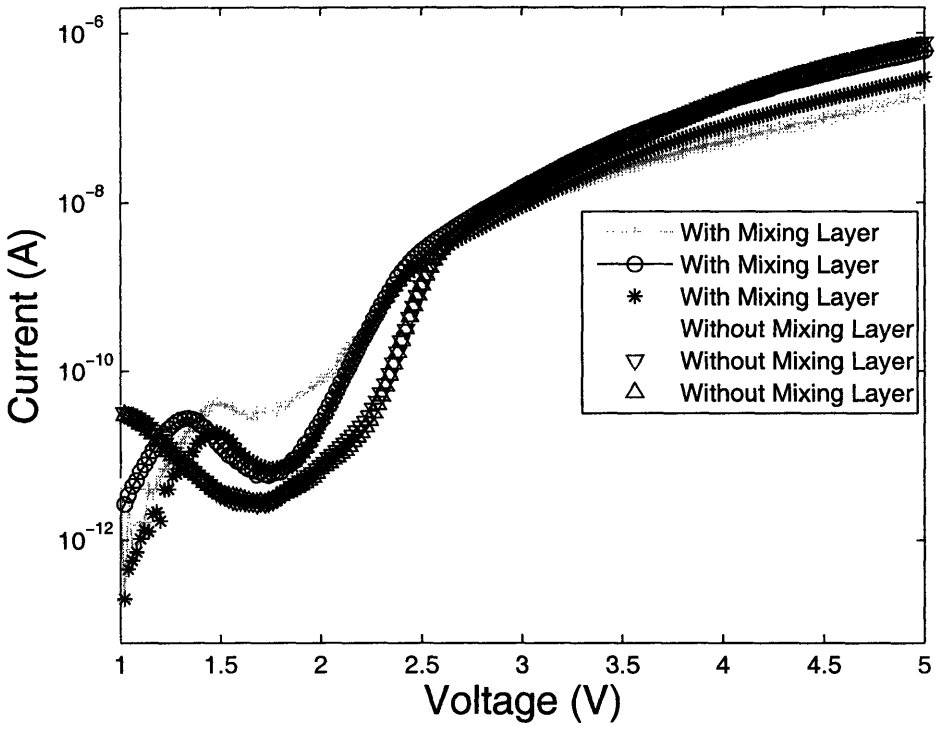

Figure 5-2: Current-voltage characteristics for three devices with and three devices without a 150$\AA$ mixing layer of FIrpic. The portion in which the current rises quickly represents recombination; the high-voltage portion represents injection-limited current.

spectral components with different local environments – one from the interface with the phosphor, and one from the bulk of the emissive layer. Devices with a 550$\AA$ thick emissive layer, both with and without the mixing layer, produce spectra that are redshifted relative to devices with the thinner emissive layer giving some credence to this idea. We can then hypothesize that for devices with a mixing layer, the interfacial spectral component is enhanced in efficiency, while the bulk component is not. It becomes difficult, however, to discern whether the enhanced efficiency measured in the devices with the mixer layer results from 1) an enhancement (because of a high value of χ_S) of the interfacial emission, which occurs at a different wavelength from the bulk emission or 2) an increased fraction of emission from the interface, which could emit more efficiently than the bulk.

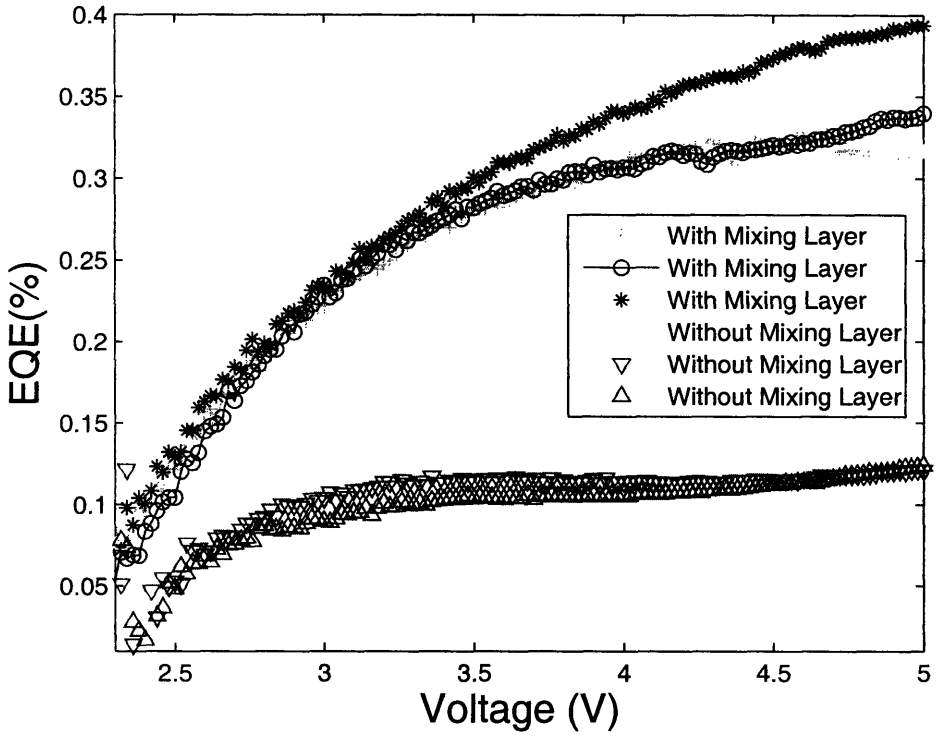

Figure 5-3: Efficiency as a function of voltage for three devices with and three devices without a 150$\mathring{A}$ mixing layer next to the emissive layer. Devices with a mixing layer show a (2.5 ± 0.3) times greater efficiency than those without the mixing layer.

A measurement of photoluminescent spectra can shed some light on which of these explanations might be correct. Photoluminescent spectra result from direct excitation of the S_1 state; therefore, we do not expect to χ_S to vary from the statistical limit of 0.25 with or without a mixing layer. Measurements with the same integration time for each device show similar spectral shifts for a thin emissive layer (and identical spectra for thick emissive layers), which seem to indicate that the mixing layer's presence increases the fraction of emission from the interface, making explanation 2) plausible. However, the intensity of the spectra with equal emissive layer thicknesses, measured for identical integration times, indicate that the photoluminescent efficiency of devices with and without the mixing layer is the same, meaning that the efficiency enhancement measured under EL might indeed be a result of explanation 1). Additionally, the EL spectra are blueshifted from the PL spectra as we would expect from

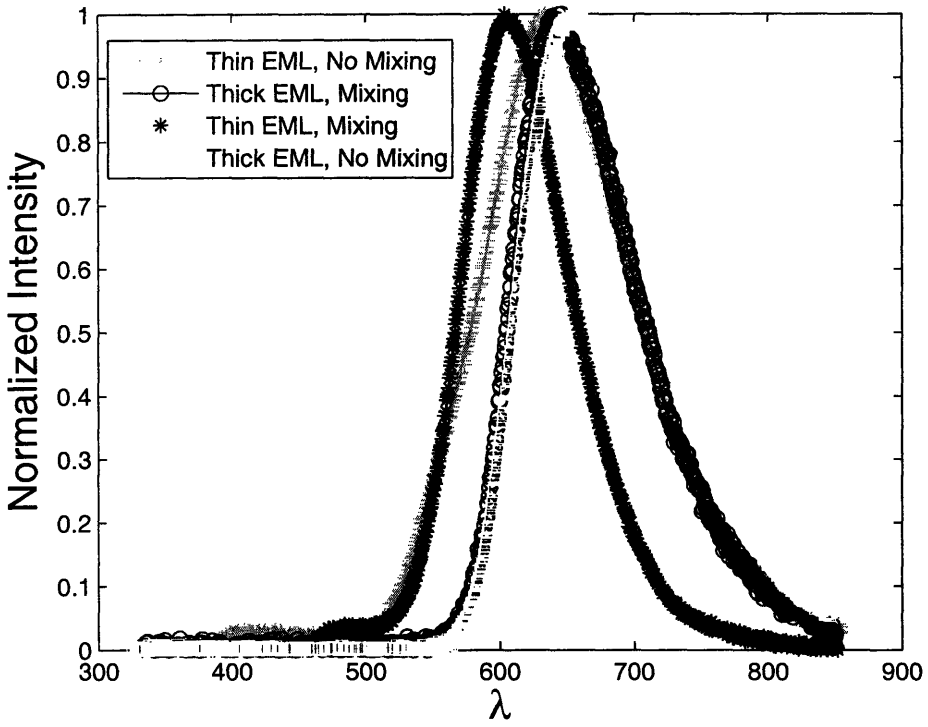

Figure 5-4: Electroluminescent spectra from devices with and without mixing layers, and of thin and thick emissive layer thickness. Thicker layers redshift compared to thinner layers; devices with a mixing layer redshift compared to those without. 'EML' designates the emissive layer.

explanation 1), as increased χ_S from the FIrpic layer would enhance emission at the interface.

Though the evidence seems to point more to explanation 2), in which the singlet fraction χ_S exceeds 0.25 leading to enhanced interface emission and efficiency, it is more desirable to work in a system in which spectral emission is identical in both the more efficient device and the control device. Additionally, working in a system with higher overall efficiency would make observation of an efficiency enhancement more obvious; it is also more interesting technologically. We describe such a system in the next chapter.

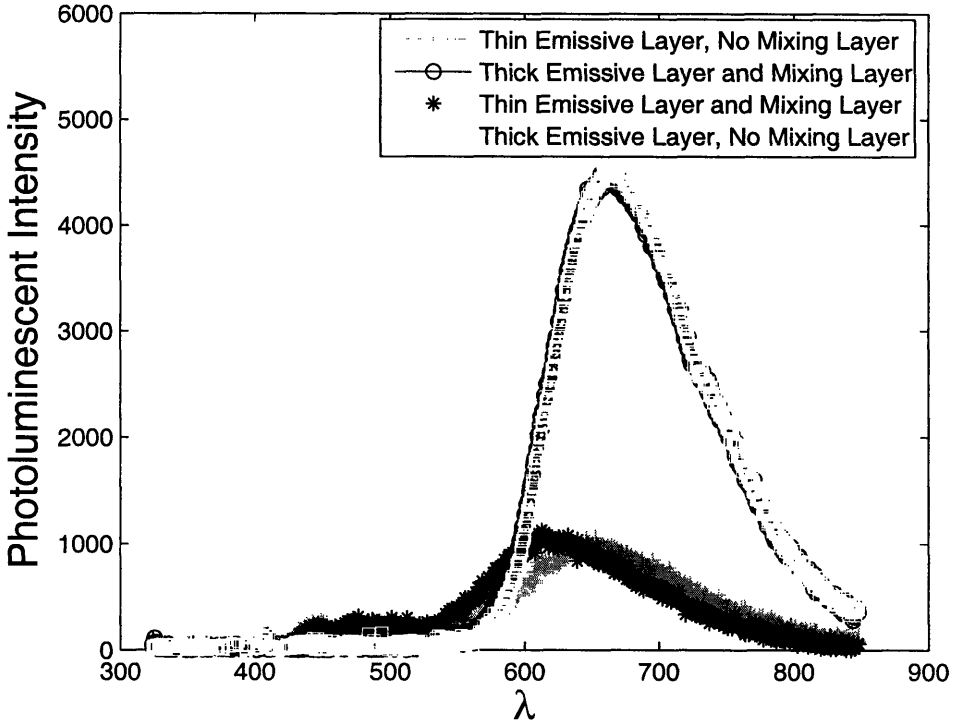

Figure 5-5: Photoluminescent spectra for devices with and without mixing layers, and of thin and thick emissive layer thickness. A device with a thin emissive layer shows higher wavelength emission in a structure with a mixing layer. For a given thickness of emissive layer, photoluminescent intensity appears to be the same with and without a mixing layer.

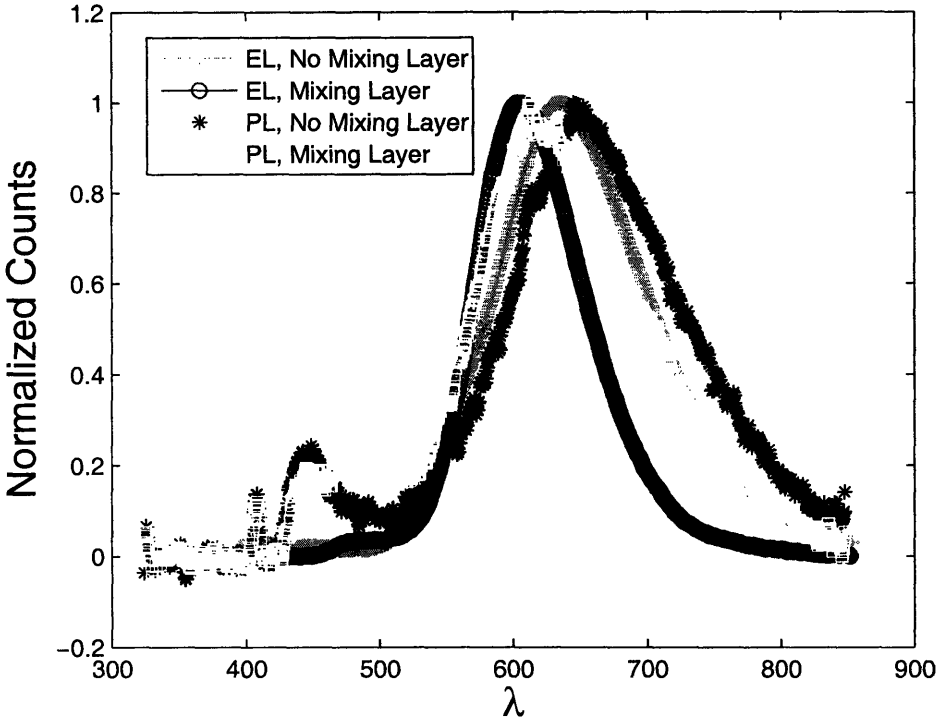

Figure 5-6: Comparison of electroluminescent and photoluminescent spectra for devices with thin emissive layer. In both cases, the devices with the mixing layer have spectra that are blueshifted compared to those without. EL spectra appear blueshifted compared to PL spectra. Spectra are plotted with 5-point smoothing for better resolution of PL data.

Chapter 6

Building a Better OLED

To improve upon the device architecture of the previous chapter and clarify the cause of the efficiency enhancement, we now change several elements of the device design. First, rather than having a neat emissive layer of the fluorophore, we dope the fluorescent dye into a host at 1.6% molar concentration. This reduces the lifetime of fluorophore, making intersystem crossing less likely. By lightly doping the host CBP with DCM2, we also hope to avoid the spectral shifts in the previous system that were hypothesized to come from emission at different locations within the neat emissive layer. We use the combination of CBP and DCM2 because the highest occupied molecular orbital is sufficiently deep compared to that of DCM2 that we can expect holes to be carried and excitons to form on the DCM2, rather than the CBP host.

In this new structure, the electroluminescent spectra shown in Figure 6-1 of devices with and without the mixing layer show a very close degree of similarity, indicating that we have overcome the difficulties of interpreting spectral shifts faced in the previous chapter.

As in the previous structure, we again see an enhancement in the efficiency, as shown in Figure 6-2 for the device with the mixing layer. The device with the mixing layer has a peak efficiency of 3.4%. The statistical average across 9 devices is measured as $(3.2 \pm 0.2)\%$, (2.7 ± 0.2) times higher than that of the statistical average across six control devices (with efficiency $(1.2 \pm 0.1)\%$), and is higher than has been previously reported for DCM2, except through sensitized fluorescence, where it was measured to

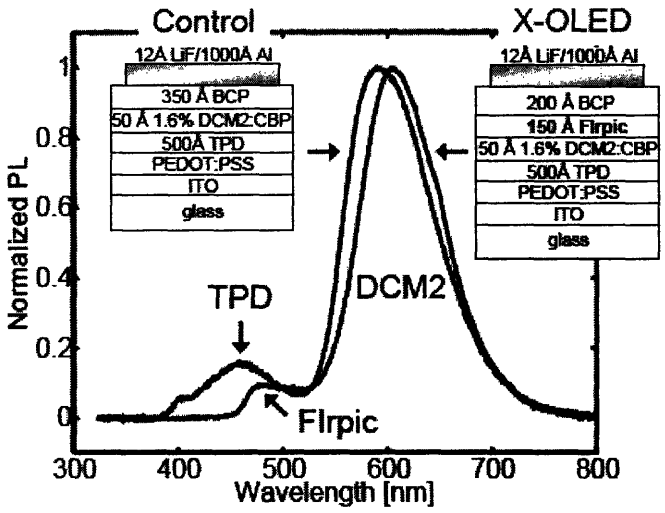

Figure 6-1: Electroluminescent structure and spectra of devices with (X-OLED) and without (Control) mixing layer. In both, emission occurs primarily from DCM2, with a center wavelength of approximately 600 nm.

be 3.3%. DCM2 doped into CBP has previously been measured to give 1% efficiency with 1% concentration doping into CBP[10], consistent with our measurement of the device without a mixing layer.

It is now left to interpret the reason for the efficiency enhancement. Three plausible reasons are: 1) Excitons form directly on FIrpic, then both singlet and triplet excitons transfer to DCM2 where it radiates (sensitized) fluorescence. Though energetically, we expect excitons to form on DCM2, the close match between our measured efficiency and that from sensitized fluorescence of DCM2 makes this explanation hard to neglect without further scrutiny. 2) FIrpic transports electrons with a different mobility than BCP, resulting in a change in the recombination zone location or change in charge balance that could affect the efficiency. 3) The FIrpic layer provides an element to mix the CT states, resulting in a singlet formation fraction much greater than in the device without a mixing layer.

To test the first explanation, we use a streak camera to measure the lifetime of the emission. In sensitized fluorescence, light emitted from both the phosphor and fluorescent dye has the lifetime of the phosphor. In our device, however, emission

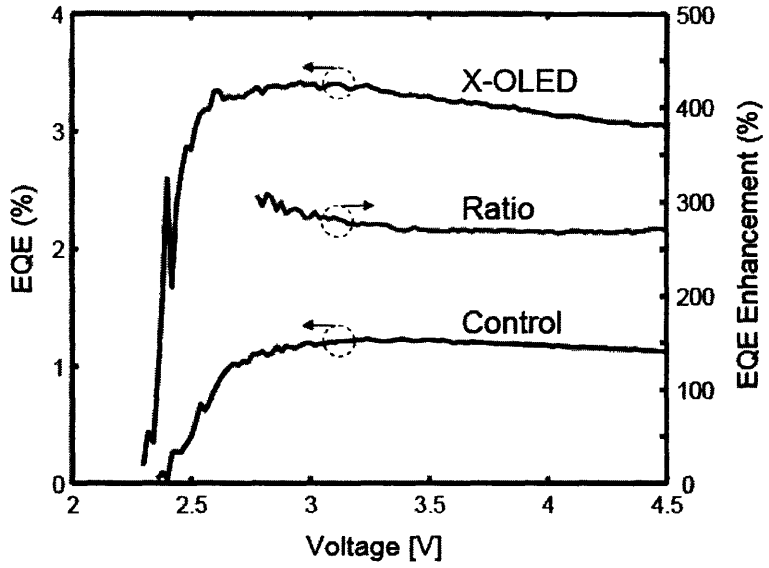

Figure 6-2: The peak external quantum efficiency of the device with the mixing layer (X-OLED) is enhanced by a factor of 2.8 relative to the device without a mixing layer (Control) for the highest efficiency device of each type.

at the wavelengths of both FIrpic and DCM2 is measured to have a lifetime of less than 70 ns, far less than the $25\mu s$ natural lifetime of FIrpic. The more than hundred-fold decrease in the lifetime of FIrpic we measure is substantially more than the previously measured[10, 42] five-fold reduction in the lifetime of $Ir(ppy)_3$ from energy transfer to DCM2 (and $Irppy_3$ emits closer to the DCM2 absorption peak than FIrpic does). In conjunction with energetic arguments, the sharp decrease in lifetime makes it unlikely that our efficiency enhancement is attributable to sensitized fluorescence; the more likely explanation for the low FIrpic lifetime is that FIrpic triplets are strongly quenched.

To test the second possible explanation, we move the $150\mathring{A}$ layer of FIrpic away from the emissive layer, placing it $100\mathring{A}$ away from the cathode and $100\mathring{A}$ away from the emissive zone, as charge transport and balance effects for the layer should be the same regardless of where it is placed. The large drop in efficiency to below 1%,

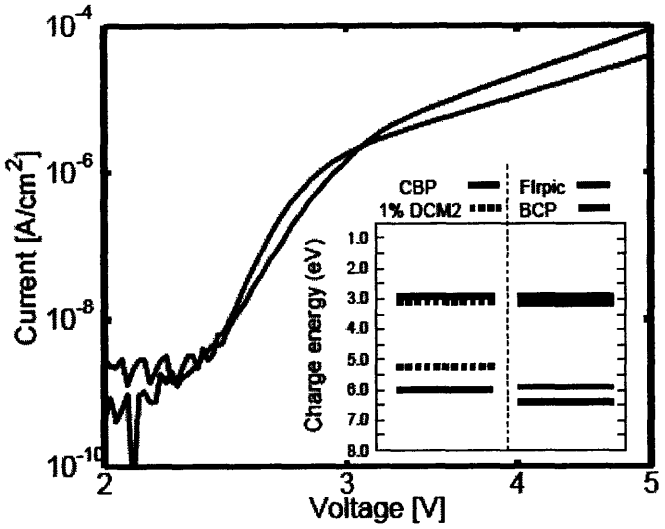

Figure 6-3: Current-voltage characteristics of the X-OLED and control OLED. The inset shows the energy level structure of the recombination interface, as measured in [19, 20, 29], showing that DCM is expected to carry holes and FIrpic electrons.

however, means that this does not explain the high efficiency we see when the mixing layer is placed next to the emissive layer. Additionally, as shown in Figure 6-3, the device with the mixing layer next to the emissive layer shows higher efficiency both where its current is higher and lower than that of the device with mixing layer spatially removed from the emissive layer.

Finally, we are left with the possibility that the enhanced efficiency is the result of an increase in χ_S from mixing in the CT-states because of the FIrpic layer. Such an explanation would indicate that χ_S=0.7 in this system.

Chapter 7

Conclusions

In this thesis, two OLED structures have been examined, each providing evidence that the efficiency of the OLED can be enhanced by the use of a heavy metal-containing material that mixes the charge-transfer state. The neat DCM/FIrpic OLED structure was found to show a (2.5 ± 0.3) times enhancement in the efficiency compared with an OLED without the heavy-metal layer. However, differences in the electroluminescent emission spectra made attributing this result to spin statistics alone a bit difficult. In the DCM2-doped CBP emissive layer/FIrpic electron transport layer, we calculate a (2.7 ± 0.2) times enhancement in the efficiency as compared to the structure without the FIrpic layer; this time, the spectral data is more straightforward.

Further study of the results described in this thesis could help clarify and further test the general model proposed in Figure 5-1 for mixing of the CT states and minimization of the intersystem crossing to achieve high efficiency. A calculation of the CT singlet-triplet energy splitting would help confirm or deny the hypothesis of mixing between the CT states, as would a measurement of the relative singlet and triplet exciton formation rates. Additionally, a measurement of the relative strength of intersystem crossing as a function of spatial separation from emitting molecules could be made by doping FIrpic into the DCM2:CBP emissive layer described earlier. Based on our model, the expectation would be that intersystem crossing would dominate over mixing of the CT-states, decreasing the efficiency. Similarly, a measurement of χ_S in the highly efficient DCM2:CBP/FIrpic OLED would further support or deny

the model proposed.

But even without these additional experiments, the results of this work indicate the first evidence that small molecule organic LEDs might be able to exceed the 25% spin statistical limit of the singlet fraction. In turn, this work has also shown that through breaking this limit, it is possible to enhance the efficiency of the OLED with a heavy-metal transport layer, whereas this was previously only possible through triplet harvesting or sensitized fluorescence with an emissive phosphor. The result can then be seen as a significant lightening of the parameters necessary to generate efficient OLED emission, in particular when considering that there are generally fewer phosphors, particularly in the deep blue, with desirable emission characteristics than there are fluorophores.

Appendix A

OLED Materials

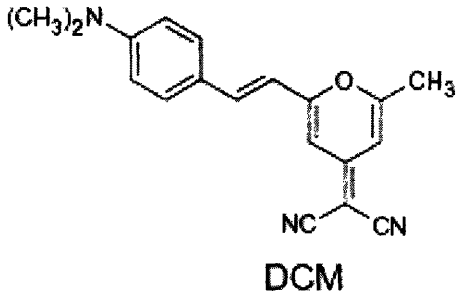

DCM

Figure A-1: 4-(dicyanomethylene)-2-methyl-6-(*p*-dimethylaminostyrl-4H-pyran (DCM). From [31].

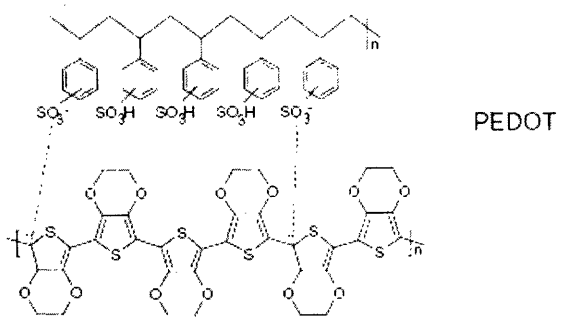

Figure A-2: poly-3,4-ethylenedioxythiophene. From [31].

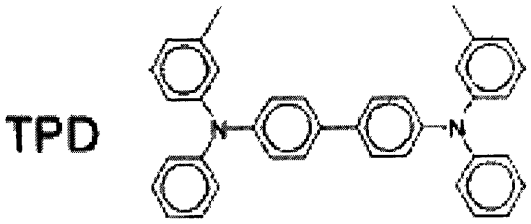

Figure A-3: N,N'-diphenyl-N,N'-bis(3-methylphenyl)-[1,1'-biphenyl] 4,4'-diamine (TPD). From [5].

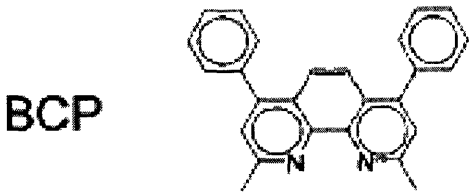

Figure A-4: 2,9-dimethyl-4,7-diphenyl-1,10-phenanthroline (BCP). From [5].

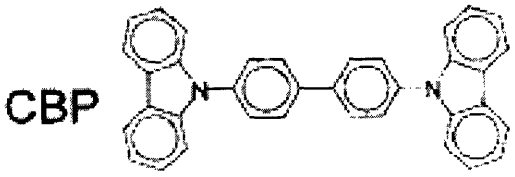

Figure A-5: 4,4'-N,N'-dicarbazolyl-biphenyl (CBP). From [5]

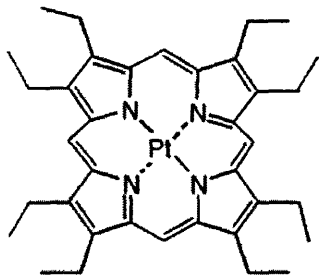

PtOEP

Figure A-6: 2,3,7,8,12,13,17,18-octaethyl- 21H,23H-porphine platinum(II) (PtOEP). From [24].

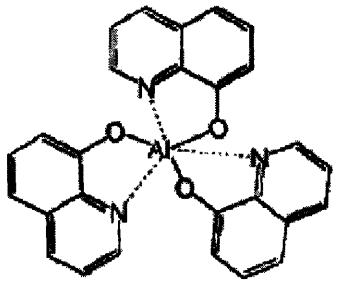

Alq_3

Figure A-7: tris-(8-hydroxyquinoline) aluminium (Alq3). From[24]

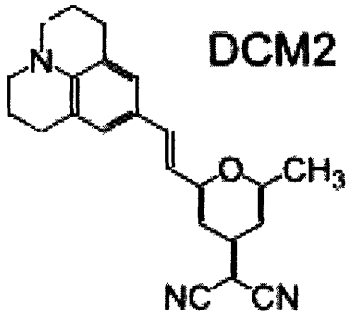

Figure A-8: tris-([2-methyl-6-[2-(2,3,6,7-tetrahydro-1H,5H-benzo[ij]quinolizin- 9-yl) ethenyl]-4H-pyran-4-ylidene]propane-dintrile) propane-dinitrile (DCM2). From[9]

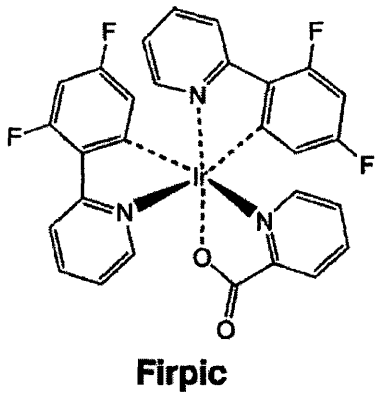

Figure A-9: iridium(III)bis[(4,6-difluorophenyl)-pyridinato-N,$C^{2'}$]picolinate (FIrpic). From [21].

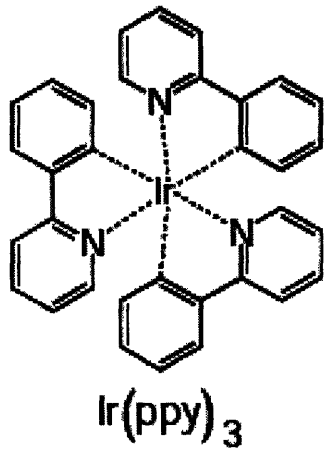

Figure A-10: *fac* tris(2-phenylpyridine) iridium (Irppy). From [10].

Bibliography

[1] Mit 8.421 course notes, 2006.

[2] P.W. Atkins and R.S. Friedman. *Molecular Quantum Mechanics.* Oxford, 2003.

[3] M. Baldo and M. Segal. Phosphorescence as a probe of exciton formation and energy transfer in organic light emitting diodes. *Phys. Stat. Sol. A*, 6:1205–1214, 2004.

[4] M.A. Baldo. *The Electric and Optical Properties of Amorphous Organic Semiconductors.* PhD thesis, Princeton University, 2001.

[5] M.A. Baldo and S.R. Forrest. Transient analysis of organic electroluminescence: I. transient analysis of triplet energy transfer. *Phys. Rev. B*, 62(16):10598–10966, 2000.

[6] M.A. Baldo and S.R. Forrest. Interface-limited injection in amorphous organic semiconductors. *Phys. Rev. B*, 64:085201, 2001.

[7] M.A. Baldo, D.F. O'Brien, M.E. Thompson, and S.R. Forrest. Excitonic singlet-triplet ratio in a semiconducting organic thin film. *Phys. Rev. B*, 60(20):14422–14428, 1999.

[8] M.A. Baldo, D.F. O'Brien, Y.You, A. Shoustikov, S. Silbey, M.E. Thompson, and S.R. Forrest. Highly efficient phosphorescent emission from organic electroluminescent devices. *Nature*, 347:151–154, 1998.

[9] M.A. Baldo, Z.G. Soos, and S.R. Forrest. Local order in amorphous organic molecular thin films. *Chem. Phys. Lett.*, 347:297–303, 2001.

[10] M.A. Baldo, M.E. Thompson, and S.R. Forrest. High-efficiency fluorescent organic light-emitting devices using a phosphorescent sensitizer. *Nature*, 403:750–753, 2000.

[11] D. Beljonne, A. Ye, Zhigang Shuai, and J. Bredas. Chain-length dependence of singlet and triplet exciton formation rates in light-emitting diodes. *Adv. Funct. Mater.*, 14(7):684–692, 2004.

[12] V. Bulovic, V.B. Khalfin, G. Gu, P.E. Burrows, D.Z. Garbuzov, and S.R. Forrest. Weak microcavity effects in organic light-emitting diodes. *Phys. Rev. B*, 58(7):3730–3740, 1998.

[13] A.L. Burin and M.A. Ratner. Spin effects on the luminescence yield of organic light emitting diodes. *J. Chem. Phys.*, 109(14):6092–6102, 1998.

[14] J.H. Burroughes, D.D.C. Bradley, A.R. Brown, R.N. Marks, K. Mackay, R.H. Friend, P.L. Burns, and A.B. Holmes. Light-emitting diodes based on conjugated polymers. *Nature*, 347:539–541, 1990.

[15] Y. Cao, I.D. Parker, G. Yu, C. Zhang, and A.J. Heeger. Improved quantum efficiency for electroluminscence in semiconducting polymers. *Nature*, 397:414–417, 1999.

[16] Wolfgang Demtroder. *Atoms, Molecules, and Photons.* Springer, 2006.

[17] S. Gasiorowicz. *Quantum Physics.* 3 edition.

[18] D.J. Griffiths. *Introduction to Quantum Mechanics.* Prentice Hall, 2005.

[19] Y. Hamada, H. Kanno, T. Tsujioka, H. Takahashi, and T. Usuki. Red organic light-emitting diodes using an emitting assist dopant. *Appl. Phys. Lett.*, 75:1682–1684, 1999.

[20] I.G. Hill and journal = J. Appl. Phys. year = 1999 volume = 86 pages = "4515-4519" A. Kahn, title = Organic semiconductor heterointerfaces containing bathocuproine.

[21] R.J. Holmes, S.R. Forrest, Y.-J. Tung, R.C. Kwong, J.J. Brown, S. Garon, and M.E. Thompson. Blue electrophosphorescence using exothermic host-guest energy transfer. *Appl. Phys. Lett*, 82(15):2422–2424, 2003.

[22] T. Hong and H. Meng. Spin-dependent recombination and electroluminscence quantum yield in conjugated polymers. *Phys. Rev. B*, 63:057402, 2001.

[23] G. Hughes and M. Bryce. Electron-transporting materials for organic electroluminiscent and electrophosphorescent devices. *J. Mater. Chem.*, 15:94–107, 2005.

[24] L.S. Hung and C.H. Chen. Recent progress of molecular organic electroluminescent materials and devices. *Mat. Sci. and Eng. R*, 39:143–222, 2002.

[25] S. Mazumdar K. Tandon, S. Ramasesha. Electron correlation effects in electrn-hole recombination in organic light-emitting diodes. *Phys. Rev. B*, 67:045109, 2003.

[26] A. Kadashchuk, A. Vakhnin, I. Blonski, D. Beljonne, Z. Shuai, J.L. Bredas, V.I. Arkhipov, P. Heremans, E.V. Emelianova, and H. Bassler. Singlet-triplet splitting of geminate electron-hole pairs in conjugated polymers. *Phys. Rev. Lett.*, 93(6):068803, 2004.

[27] S. Karabunarliev and E.R. Bittner. Spin-dependent electron-hole capture kinetics in luminescent conjugated polymers. *Phys. Rev. Lett.*, 90(5):075026, 2003.

[28] A. Kohler and J. Wilson. Phosphorescence and spin-dependent exciton formation in conjugated polymers. *Organic Electronics*, 4:179–189, 2003.

[29] G. Lei, L. Wang, and Y. Qiu. Multilayer organic electrophosphorescent white light-emitting diodes without exciton-blocking layer. *Appl. Phys. Lett.*, 88:103508, 2006.

[30] G. Li, C.H. Kim, P.A. Lane, and J. Shinar. Magnetic resonance studies of tris-(8-hydroxyquinoline) aluminum-based organic light-emitting devices. *Phys. Rev. B*. 69:165311, 2004.

[31] J. Tardy M. Ben Khalifa, D. Vaufrey.

[32] N.K. Patel, S. Cina, and J.H. Burroughes. High-efficiency organic light-emitting diodes. *IEEE Journal on Selected Topics in Quantum Electronics*, 8(2):346–361, 2002.

[33] M. Reufer, M.J. Walter, P.G. Lagoudakis, A.B. Hummel, J.S. Kolb, H.G. Roskos, U. Scherf, and J.M. Lupton. Spin-conserving carrier recombination in conjugated polymers. *Nature Materials*, 4(4):340–346, 2005.

[34] J.J. Sakurai. *Modern Quantum Mechanics.* Addison-Wesley, 1994.

[35] G. Sauerbrey. Verwendung von schwingquarzen zur wgung dnner schichten und zur mikrowgung. *Z. Phys.*, 155:206, 1959.

[36] M. Schott. Introduction to the physics of organic electroluminescence. *Comptes Rendus de l'Academic des Sciences Serie IV Physique Astrophysique*, 1(4):381–402, 2000.

[37] J.C. Scott. Metal-organic interface and charge injection in organic electronic devices. *J. Vac. Sci. Technol. A*, 21(3):521–531, 2003.

[38] M. Segal, M.A. Baldo, R.J. Holmes, S.R. Forrest, and Z.G. Soos. Excitonic singlet-triplet ratios in molecular and polymeric organic materials. *Phys. Rev. B*, 68:075211, 2003.

[39] Z. Shuai, D. Beljonne, R.J. Silbey, and J.L. Bredas. Triplet exciton formation rates in conjugated polymer light-emitting diodes. *Phys. Rev. Lett.*, 84(1):131–134, 2000.

[40] C.W. Tang and S.A. VanSlyke. Organic electroluminscent diodes. *Appl. Phys. Lett.*, 51(12):913–915, 1987.

[41] Nicholas J. Turro. *Modern Molecular Photochemistry.* University Science, 1991.

[42] P.E. Burrows V.B. Khalfin J. Wang S.Y. Chou V.G. Kozlov, G. Parthasarathy and S.R. Forrest. Structures for organic diode lasers and optical properties of organic semiconductors under intense optical and electrical excitations. *IEEE Journal of Quantum Electronics*, 36(1):18–26, 2000.

[43] J.S. Wilson, A.S. Dhoot, A.J.A.B. Seeley, M.S. Khan, A. Kohler, and R.H. Friend. Spin-dependent exciton formation in π-conjugated compounds. *Nature*, 413:828–831, 2001.

[44] M. Wohlgenannt, K. Tandon, S. Mazumdar, S. Ramasesha, and Z.V. Vardeny. Formation cross-setions of singlet and triplet excitons in π-conjugated polymers. *Nature*, 409:494–496, 2001.

[45] A. Ye, Z. Shuai, and J.L. Bredas. Coupled-cluster approach for studying the singlet and triplet exciton formation rates in conjugated polymer led's. *Phys. Rev. B*, 65(4):045208, 2002.